Progress In Electromagnetics Research, PIER 64, 23–42, 2006

DIVERSITY TECHNIQUES WITH PARALLEL DIPOLE ANTENNAS: RADIATION PATTERN ANALYSIS

A. Khaleghi

Electromagnetic Department
Supelec, 3, rue Joliot-Curie Plateau de Moulon
91192, Gif sur Yvette, France

Abstract—Two parallel dipoles are assessed for antenna diversity. The three-dimensional radiation pattern is considered for signals correlation coefficient. The pattern analysis reveals that, depending on dipole spacing, three types of diversity techniques are generated: space, amplitude-pattern and phase-pattern diversity. The weighting of each technique in signals correlation coefficient mitigation is investigated. The results show that for closely spaced dipoles, the generated phase-pattern diversity is the most dominant factor which greatly reduces the signals correlation coefficient.

The diversity configuration is measured in a rich scattering environment. Results include signals correlation coefficient, diversity gain for selection combining and maximum ratio combining, effective diversity gain and antenna radiation efficiency can be demonstrated. We show that in rich multipath channel the minimum spatial distance, for effective diversity gain performance, is reduced from 0.5λ for uncoupled dipoles to 0.15λ for coupled dipoles.

1. INTRODUCTION

Antenna diversity plays a crucial role in wireless communications over fading channels being the topic of considerable research for many decades [1]. In recent days, there has been increasing use of antenna diversity in mobile terminals and in indoor small base stations. In indoor environments, the angular spread of scattering field on the antennas is large and gives short spatial de-correlation distance. The diversity performance in such multipath environment depends directly on the antennas de-correlation distance [2]. The trend of recent development on the small communication devices is to design closely spaced antenna elements to achieve an effective diversity system

within the available small space. The resulting closely spaced antenna elements exhibit mutual coupling [3]. The antenna de-correlation distance is significantly affected by the mutual coupling. Measurements in the past [1] and our recent research [4] show that closely spaced dipole antennas (0.05 wavelengths apart) can still give a low signals correlation, in contrast to previous work on uncoupled dipoles showing that 0.5 wavelengths spacing is needed.

A variety of studies has analytically examined the diversity performance of coupled antennas. These studies are performed in two categories: one considers the mutual impedance, mutual coupling or scattering parameters of the antennas [5–8] and the others insist on the effect of coupling on the antenna radiation pattern and the resulting correlation between the received signals [9–14]. The available analytical models based upon the mutual impedance provide an approximation of the diversity performance. This is because that we do not know the exact current distribution along the coupled antennas [6]. An alternative method is to consider the diversity performance using embedded element pattern defined in [14]. The present paper gives a detail analysis of the correlation coefficient of two parallel dipoles with various spacing. We treat the same geometry used by Kildal and Rosengren [13], but we use a numerical approach instead of their classical method. Our analysis based upon the complex pattern shows a composite form of the space and the pattern diversity for the dipole spacing less than 0.4λ. A rigorous analysis of the radiation pattern divides the pattern diversity into amplitude-patterns and phase-patterns diversity. The relative impacts of these diversity techniques on the signals correlation coefficient are separately investigated. It is shown that, the phase-patterns diversity is the most dominant factor in correlation mitigation for small dipole spacing. It is also shown that the patterns can have very similar shapes and still be uncorrelated if the phase-patterns are different.

The simulations are followed by laboratory measurements carried out inside a reverberation chamber [15]. We use Supelec large reverberation chamber as a facility for testing the diversity antennas [16]. The dimensions of the chamber are 3 meters long, 1.80 meters wide and 2.80 meters high. The chamber makes use of a mechanical stirrer. The measurements are performed at 2450 MHz with two half-wave dipoles. The signals correlation coefficient is precisely measured with high spatial resolution. The selected high frequency and the large chamber size make the measurement accuracy good. The apparent diversity gains for the selection combining (SC) and the maximum ratio combining (MRC) versus dipoles separations are computed from the measured complex signals. The measured apparent diversity gain

illustrates some variations (± 0.5 dB) in small antenna separation that is explained in Section 3.3. Effective diversity gain which represents the gain over a single antenna and includes the effect of both correlation coefficient and radiation efficiency is also measured by the same manner explained in [13]. The mean received power degradation at the coupled dipoles is measured and is compared with the modeled radiation efficiency.

2. CORRELATION COEFFICIENT AND PATTERN ANALYSIS

The signals correlation between two antenna configurations is a performance factor that shows the diversity effects of multiple antennas. In Rayleigh fading channel the complex correlation coefficient (ρ_c) is given by [1, 17, 18]

$$\rho_c = \frac{\int\limits_{\Omega} \left(\frac{X}{1+X} E_{1\theta} E_{2\theta}^* P_\theta + \frac{1}{1+X} E_{1\varphi} E_{2\varphi}^* P_\varphi \right) d\Omega}{\left(\sqrt{\int\limits_{\Omega} \left(\frac{X}{1+X} E_{1\theta} E_{1\theta}^* P_\theta + \frac{1}{1+X} E_{1\varphi} E_{1\varphi}^* P_\varphi \right) d\Omega} \times \sqrt{\int\limits_{\Omega} \left(\frac{X}{1+X} E_{2\theta} E_{2\theta}^* P_\theta + \frac{1}{1+X} E_{2\varphi} E_{2\varphi}^* P_\varphi \right) d\Omega} \right)} \quad (1)$$

where $\Omega(\theta, \varphi)$ is the spatial angles in steradian (θ and φ are depicted in Fig. 1), $E_{1\theta}, E_{1\varphi}, E_{2\theta}$ and $E_{2\varphi}$ are the complex envelopes of the θ and φ components of the field patterns of the antenna for each port excitation; P_θ and P_φ are the probability distributions of the power incident on the antenna in the θ and φ polarizations, respectively; X is the cross polarization power ratio and is defined as the mean received power in the vertical polarization to the mean received power in the horizontal polarization. The incident field powers are normalized to unity and the antenna power gains are normalized to isotropic.

In an indoor environment and equally inside a reverberation chamber there are many nearby scatters, so the signals are arriving from more isotropically scenarios, therefore a uniform scattering field distribution is supposed [19]. To provide a good agreement with the experimental measurement setup (see Section 3), the correlation coefficient (1) is derived in an isotropically scattered field environment ($P_\theta = P_\varphi = 1/4\pi$) and unpolarized case (X=1). Then, if the antennas are vertically polarized, as is the case in parallel side-by-side and z-

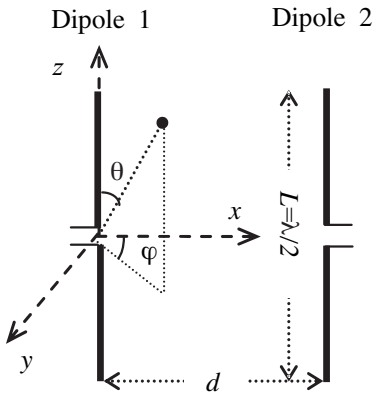

Figure 1. Two parallel (half-wave) dipoles horizontally separated with distance d.

oriented dipoles ($E_{1\varphi} = E_{2\varphi} = 0$), (1) is simplified to

$$\rho_c = \frac{1}{4\pi} \int_{\Omega} E_{1\theta}(\Omega) \cdot E^*_{2\theta}(\Omega) d\Omega = \frac{1}{4\pi} \int_{\Omega} |C(\Omega)| e^{j\Psi(\Omega)} d\Omega \qquad (2)$$

Equation (2) is also expressed as a function of the coupling-pattern magnitude and coupling-pattern phase factors, $|C(\Omega)|$ and $\Psi(\Omega)$, respectively. The envelop correlation coefficient, i.e., the correlation coefficient between signals envelop, in Rayleigh distributed multipath channels is approximately given by the square of the complex correlation [5]. We have shown that in a rich field scattering environment (i.e., reverberation chamber) the correlation coefficient of the signal powers ($\rho_{P_1P_2}$) and the signal voltages ($\rho_{V_1V_2}$) are closely equal and both satisfies [16]

$$\rho_e = \rho_{V_1V_2} = \rho_{P_1P_2} \cong |\rho_c|^2 \qquad (3)$$

The envelop correlation between two identical patterns which are circularly symmetric and horizontally separated with distance d is given by the square of the zero order Bessel function $|J_0(\beta d)|^2$, where β is the wave number. This is so called Clarke function [5, 20] and shows the spatial diversity effects. The theoretical envelop correlation between two half-wave dipoles (Fig. 1), which are parallel, z-oriented and horizontally separated with distance d, is computed from the dipole antenna element factor ($|E_{1\theta}| = |E_{2\theta}| = A\cos(\pi/2\cos\theta)/\sin\theta$) and the coordinate translation term ($\Psi(\Omega) = \beta d\cos\varphi\sin\theta$) by applying into (2) and (3). Fig. 2 shows the theoretically calculated envelop

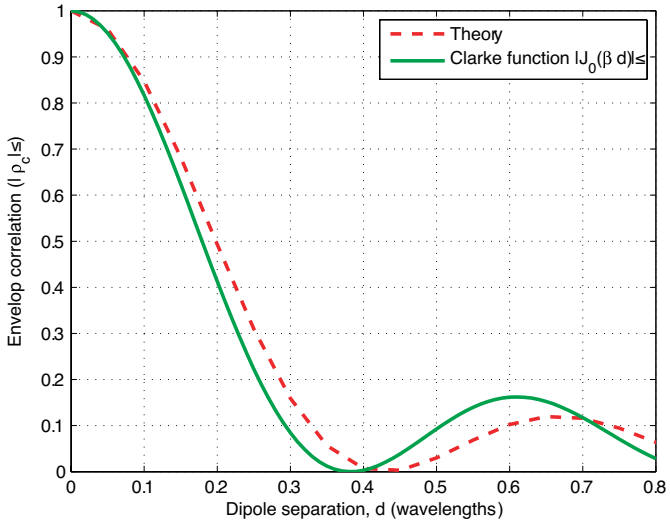

Figure 2. (- - -) Theoretical envelop correlation between two half-wave dipoles with separation distance d, computed from the antenna element factor by assuming an isotropically scatters; (—) Clarke's function.

correlation coefficient against distance. The calculated result is similar to the Clarke function. As a point to note, the curve will be the same as Clarke function when the scattered field is uniformly distributed in the antenna azimuth plane.

The signals correlation coefficient varies in the same manner with antenna separation if no mutual coupling effect between the antennas is assumed [5]. In practical diversity applications, the antennas are both matched to 50Ω source impedances. When the antennas are brought closer, the mutual coupling between the antennas is increased [4]. As a result, the coupling alters somewhat the current (amplitude and phase) along the antennas. The direct result of the new current distribution is a modified radiation patterns, lead to a novel form of diversity in addition to the space diversity. To examine the impact of the generated diversities on the correlation coefficient, no expressions for the coupled antenna patterns exist, motivating the use of full-wave electromagnetic solutions.

The dipole antenna configuration (Fig. 1) is simulated using time-domain transmission line matrix (TD-TLM) method code. The TLM method is a three-dimensional volumetric time domain method that provides a full temporal field solution to the Maxwell equations. In this analysis, two half-wave dipoles are horizontally separated with distance

d and one is located at the centre of the computational domain. The simulated dipoles radius is 1.2 mm i.e., 0.01λ for 2450 MHz. Because we are considering narrow-band systems, single-frequency antenna excitation is assumed. The TLM grid uses 88 cells per wavelength in z-direction and 160 cells per wavelength in x and y directions. This fine grid resolution permits the accurate calculation of the dipoles currents at very close spacing.

The radiation field pattern of the antennas is complex value and can be expressed as field amplitude and phase in relation to the spatial angles, $\Omega(\theta, \varphi)$. The 3-D complex embedded element pattern of each dipole by assuming the next dipole is Z_0 terminated (for instance, $Z_0 = 50\Omega$) is computed in amplitude and phase, separately. Using the numerical analysis code, accurate estimation of the antenna currents at the presence of the coupling is obtained and a rigorous value of the patterns are computed. The numerically computed complex patterns are applied into (2), (3) and the envelop correlation coefficient is derived. The simulated envelop correlation against distance is depicted in Fig. 3. Small envelop correlation is illustrated even for small apart, for instance for $d = 0.05\lambda$ gives $\rho_e = 0.35$. As shown, the envelop correlation, for small antenna separations, is significantly reduced compared to the theoretical value (see Fig. 2 and Fig. 3). This indicates that the assumption that the patterns are identical and circularly symmetric is no longer suitable when we calculate the embedded element patterns.

Here we explain the observed low signals correlation by the analysis of the farfield pattern. The radiation field amplitude and phase values, both, impact the signals correlation coefficient. To evaluate the related effects, the coupling-pattern amplitude, $|C(\Omega)|$, and the coupling-pattern phase, $\Psi(\Omega)$, are separately computed from the modeled patterns. Referring to Fig. 1 and (2), we divide the coupling-pattern phase, $\Psi(\Omega)$, into: the coordinate translation term and an assumed phase-patterns difference generated by the coupling, $\Delta\Phi(\Omega)$, i.e.,

$$\Psi(\Omega) = \beta d \cos\varphi \sin\theta + \Delta\Phi(\Omega), \quad \Omega(\theta, \varphi) \tag{4}$$

Now we consider the following cases:

1) If the dipole spacing is more than one wavelengths ($d > \lambda$), the mutual power coupling between the antennas is too small (less than -18 dB) [4]. The far-field patterns are similar. Therefore, the coupling-pattern amplitude is theoretically given by the square of the element factor of an isolated dipole (i.e., $|C(\Omega)| = [A\cos(\pi/2\cos\theta)/\sin\theta]^2$); the coupling-pattern phase is generated due to their different locations i.e., $\Delta\Phi(\Omega) = 0$ in (4). By this assumption, the signal correlation

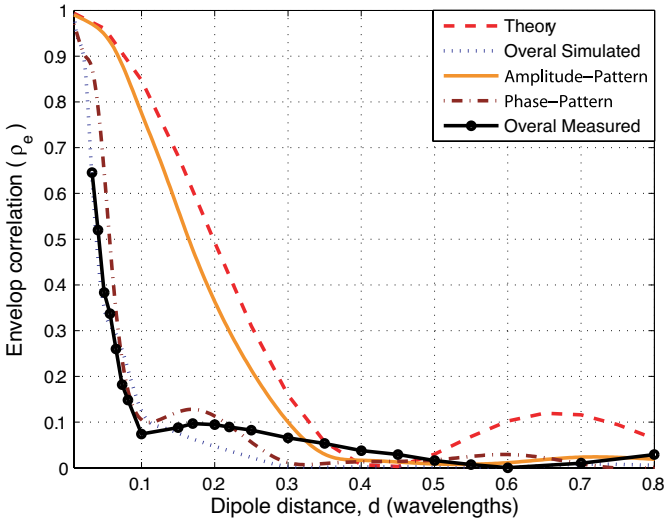

Figure 3. Correlation coefficient as a function of the dipole spacing (wavelength), simulated and measured inside an isotropically scattered field environment, (- - -) theoretical calculated; (...) overall simulated; (—) simulated using amplitude-pattern diversity effects; (-.-.-) simulated using phase-pattern diversity effects; (–●–) overall measured inside reverberation chamber.

versus dipole spacing follows the theoretical curve given in Fig. 3 and is known as the space diversity.

2) The numerically computed coupling-pattern amplitude, $|C(\Omega)|$, is replaced by the theoretical value and the coupling-pattern phase, $\Psi(\Omega)$, is supposed to be varying according to the space factor i.e., $\Delta\Phi(\Omega) = 0$ in (4). The envelop correlation versus dipole spacing is computed by (2) and (3). The result including the effects of the amplitude-pattern diversity is illustrated in Fig. 3. As shown, the correlation coefficient is slightly reduced compared to the space diversity curve. The maximum effect is observed for $d = 0.2\lambda$ and the correlation is alleviated about 0.15.

3) The numerically computed coupling-pattern phase, $\Psi(\Omega)$, is applied into (2) and the coupling-pattern amplitude is set to be equal to the theoretical value. The correlation coefficient is computed containing the effects of the assumed phase-pattern diversity, $\Delta\Phi(\Omega)$. Fig. 3 illustrates the relative effects of the phase-pattern diversity. As can be seen, due to the phase-pattern diversity the correlation coefficient for small separations is greatly reduced compared to the

theoretical curve. The maximum effect is observed for $d = 0.1\lambda$ and the correlation is reduced more than 0.7. As shown, for $d < 0.4\lambda$ the impact of the phase-pattern diversity on the correlation mitigation is stronger than the amplitude-pattern diversity.

The above analyses reveal that, the phase-pattern diversity is the most dominant factor in signals correlation mitigation in the coupled antennas. It is important to point out that in compact antenna diversity arrangement, if a significant mutual coupling exists the phase-pattern information is essential for diversity performance evaluation. The idea is effective and simplifies the design of antenna pattern-diversity systems, where low correlation coefficient is subjected to small overlapped radiation patterns and the phase-pattern diversity effect is being neglected [21–23]. To illustrate this term, the embedded element pattern of the dipole diversity configuration for two different separations ($d = 0.1\lambda$ and $d = 0.2\lambda$) are shown in Fig. 4. The farfield patterns for both cases are highly overlapped but due to the phase difference between the patterns the received signals are uncorrelated i.e., $\rho_e = 0.1$ and 0.05, respectively.

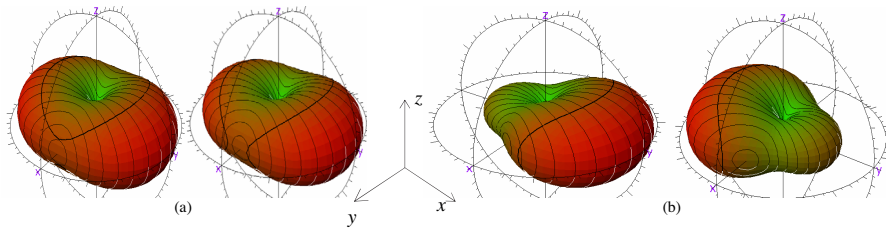

Figure 4. Embedded element patterns of two closely spaced dipole antennas for two different separation distances (a) $d = 0.1\lambda$ (b) $d = 0.2\lambda$; the bolded line shows the 3 dB beam-width. The radiation patterns are highly overlapped but the patterns are still uncorrelated.

We have shown that the composite form of the space and the phase-pattern, i.e., $\Psi(\Omega)$, diversity is the most efficient diversity techniques for the coupled dipoles. Illustration of the pure phase-pattern diversity, $\Delta\Phi(\Omega)$, requires careful simulation of the diversity antennas. We have simulated the antenna structure shown in Fig. 1 by the assumption that the excited antenna is always located at the centre of the coordinate system. This means that the pattern of the dipole 1 is computed at the presence of the dipole 2, then the pattern of dipole 2 is computed when the two antennas are repositioned i.e., dipole 2 is at the centre of the coordinate. Again the spherical field pattern will be taken, which is a mirror image of the first field pattern

in this situation. By the present approach the effect of the different locations (space diversity) is removed from the farfield patterns and the phase difference between the two simulated patterns is related to the phase-pattern diversity, i.e., $\Psi(\Omega) = \Delta\Phi(\Omega)$. Fig. 5 illustrates the spatial phases-pattern difference for $d = 0.1\lambda$ dipole spacing. In the absence of the mutual coupling, the phase-pattern difference for all spatial angles will be zero.

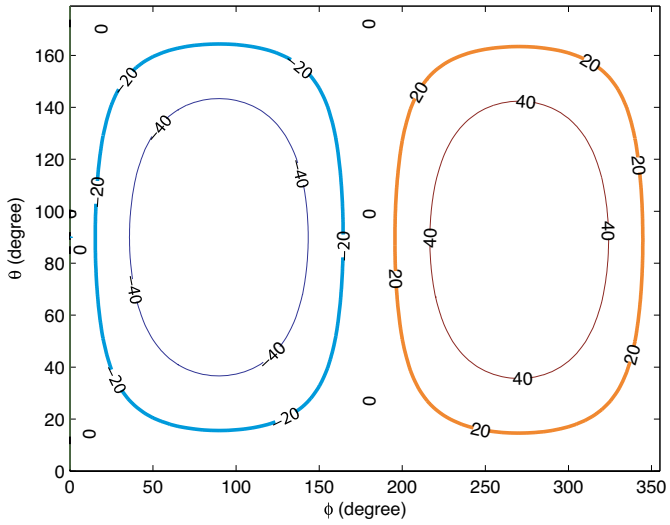

Figure 5. Illustration of the pure phase-pattern diversity, $\Delta\Phi(\Omega)$, versus spatial angles $\Omega(\theta, \varphi)$ for dipole spacing, $d = 0.1\lambda$.

3. ANTENNA MEASUREMENT

3.1. Measurement Setup

Reverberation chambers have large popularity for electromagnetic immunity testing. In recent years, there has been increasing use of reverberation chambers for wireless antenna tests in multipath environments [4, 13–16, 23]. The measurements in the present paper are performed in Supelec reverberation chamber. The measurement setup is depicted in Fig. 6. The metal walls of the chamber allow a large field to be built up inside the chamber. A large stirrer in the form of four tilted cross paddles is installed at the ceiling and stirs the cavity modes of the chamber by turning. The reverberation chamber corresponds to a spatially uniform multipath propagation channel in which all directions of arrivals are equally

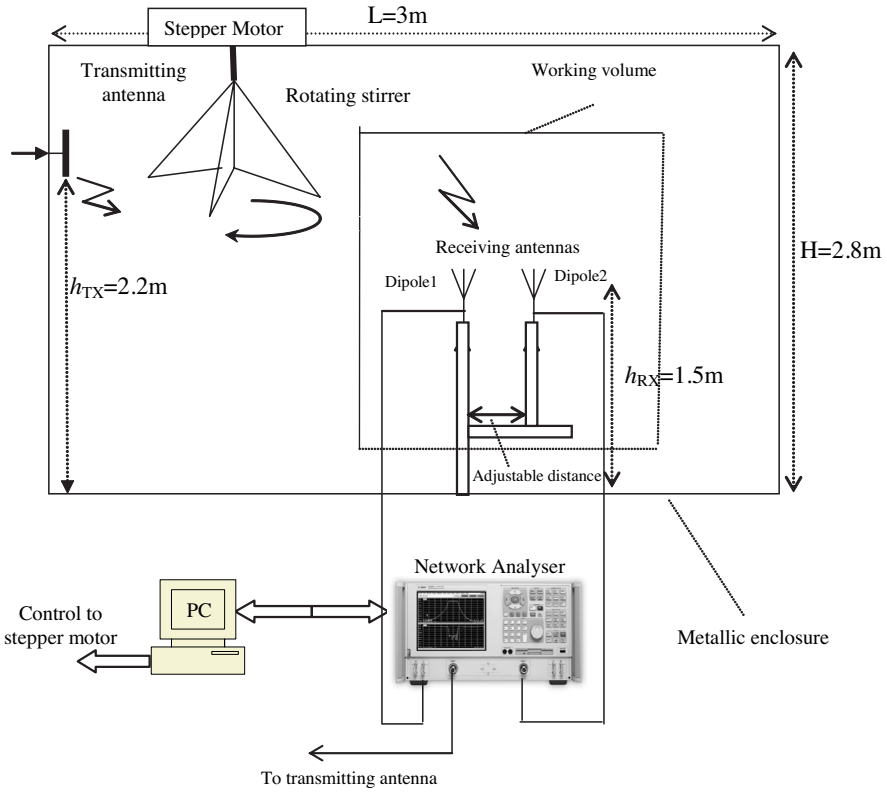

Figure 6. Experimental measurement setup for multipath generation consisted in: large reverberation chamber with one rotating stirrer; one transmitting antenna (dipole) installed on the wall at $h_{Tx} = 2.2\,\mathrm{m}$ next to the stirrer; two half-wave dipole receiving antennas with an adjustable distance; network analyser as the transmitter and receivers; personal computer for controlling the stepper motor and the data analysis.

probable [26, 27, 15]. Whenever the input field is perfectly stirred, the resulting electromagnetic field within the chamber (in one point) can be seen as the superposition of many independent plane waves from all directions and therefore the field is a complex Gaussian process. As a matter of fact the amplitude of the complex electromagnetic field is Rayleigh distributed and the phase is uniformly distributed. In the present work, to provide an environment with perfectly stirred field the transmitting antenna is a dipole, wall mounted at a height of 2.2 m and is horizontally polarized and installed at the left side of the

rotating stirrer (see Fig. 6). The receiving antennas are two similar half-wave dipoles that are fed with coaxial line through a quarter-wavelength balun. The dipoles are vertically polarized to avoid direct coupling from the transmitting antenna. They are fixed at the working volume of the chamber with sufficient distance (more than 5λ) from the stirrer and the metallic walls at a height of 1.5 m. This large distance from the surrounding metallic objects avoid the mutual effects of the environment on the antenna characteristics. An E8358A Agilent vector network analyzer is used as both transmitter and receiver, which allows coherent channel sounding. Some modifications at the network analyzer port connections are made that permits to use it as a three ports instrument, one for transmitting and the two others for receiving. It is set to work in single trace, single frequency and zero span mode that permits to acquire the received signals in time domain. The chamber is excited using a CW signal at 2450 MHz generated by the transmitter system of the network analyzer. The stirrer is programmed and is continuously rotating with a constant angular velocity of $\omega = 2\pi/100$ (rad/sec) i.e., one revolution takes 100 sec. The amplitude of the received signal is modulated due to the fading generated by the rotating stirrer. The signals amplitude variations are detected by the receiver system of the network analyzer and the signals are sampled and stored inside the internal buffer of the network. The internal buffer can record up to 1601 samples of the signals. Using the single trace mode the signal samples are recorded and then stored in an external disk for offline processing.

The first-order statistics (complex Gaussian distribution) and the second order-statistics (auto-correlation of the real and imaginary parts, cross-correlation of the real-imaginary parts, level crossing rate and average fade duration) of the measured fading signals are examined [16]. The measurement illustrates good agreement between the reverberation chamber fading emulator and the fading simulators related to Clarke [24] and Jakes [25]. The fading amplitude for one revolution of the stirrer is Rayleigh distributed. The scattered field cross-polarization ratio is unity. The measurement inside the chamber is repeatable by the stirrer revolution.

The above approach offers a reasonable measurement time for signals acquisition i.e., the measurement time for single frequency with two receiving antennas takes only 100 sec. The chamber is naturally shielded from any interfering signals through the measurements.

In the measurement procedure we have avoided the use of frequency stirring used in [13, 14]. This is because, when the frequency is changed the normalized distance between the antennas is corrupted and this gives smaller accuracy. Also the frequency stirring

makes changes in the antenna port impedances (if the antennas are narrowband) and this reduce the accuracy of the single frequency measurement. Further, small frequency stirring would not generate uncorrelated fading signal samples.

3.2. Signals Correlation Coefficient

In the diversity test procedure the dipole antennas are connected to the receivers. The complex S-parameters between the transmitter port and the dipole receiving antennas are simultaneously sampled with a rate of 1601 samples per revolution of the rotating stirrer. The sample numbers are sufficient and can describe the manner in which the multipath channel change (modulates) the transmitted signals at 2450 MHz (this can be tested through the samples autocorrelation function) [16]. The received signals are synchronized with the transmitter therefore the signals phase can be evaluated, accurately. One dipole antenna is fixed and the next one is adjustable and the distance can be varied. The distance between the parallel dipoles are adjusted from 0.025λ up to λ and the measurements are repeated for one revolution of the stirrer and for each antenna apart. In small dipole spacing more resolutions are applied. The received signals are recorded and are used for offline processing.

Considering the received signals as $x_1(t)$ and $x_2(t)$ (in complex base-band representation) the complex correlation coefficient between the signals is defined as

$$\rho_c = \frac{E\left\{(x_1(t) - \overline{x}_1)(x_2(t) - \overline{x}_2)^*\right\}}{\sqrt{E\left\{|x_1(t) - \overline{x}_1|^2\right\} E\left\{|x_2(t) - \overline{x}_2|^2\right\}}} \tag{5}$$

where E is the expectation value and the bar indicates time average. The envelope correlation coefficient between the diversity signals are computed (3). Fig. 3 shows the measured correlation coefficient against separation distance. Small correlation coefficient is measured even for small dipole spacing. The measurement and simulation results are in good accordance with a maximum error of about 0.07 for $d = 0.3\lambda$. This small discrepancy is explained by the way that, in the simulation procedure the non-exciting antenna element is locally connected to 50Ω terminal impedance, even when the antenna resonance length is moved from the exciting frequency (due to the mutual coupling). In the measurement procedure, we are not able to locally connect the dipole antennas to the 50Ω loads and they are connected through the quarter-wavelength balun to the coaxial line. The terminal loads of two dipoles, in small separations, are drifted from the 50Ω impedances (for the measurement frequency) by to the mutual coupling effects. This

generates a condition that both antennas are not locally connected to 50Ω and various terminal impedances depending on the separation distance between the antennas are generated. This term illustrates more effects on the diversity gain variations (Section 3.3).

3.3. Diversity Gain

Diversity gain is the performance factor characterizing a diversity system. It depends on the correlation coefficient, power imbalance in diversity branches and signals combining. In order to investigate the full diversity benefit, we utilize the concept of effective diversity gain introduced in [13, 14]. For present paper the diversity gain is determined from the data at 0.1 level on the diversity cumulative distribution function (CDF) and assuming SC and MRC [1]. Accurate measurement of the diversity gain in smaller levels requires large number of uncorrelated signal samples.

The CDF plot of the measured signals for various separations is computed. Fig. 7 illustrates the CDF plot of the received signal powers, P_1 and P_2 (for instance, $d = 0.2\lambda$), normalized to the mean branch power, also the CDF of signals after combining. The CDF plot of the received powers using single dipole, with no additional antenna close to it, is also plotted. The apparent diversity gain is obtained from the difference in dB between the signal powers in diversity branches and after signal combining at 0.1 CDF level. To avoid the mutual effect of the power imbalance on the diversity gain estimation, the difference in branches mean powers is verified through the measurement and lies within ± 0.3 dB interval. Fig. 8 shows the measured apparent diversity gains versus dipoles separation. As shown, the diversity gain for $d > 0.5\lambda$ is constant about 5 dB for SC and 6.5 dB for MRC. Small variations within ± 0.5 dB at close distances ($0.05\lambda < d < 0.5\lambda$) are depicted. As it was explained different terminal impedances on the various spacing are generated and the mutual effect gives diversity gain variations. The termination effects can be compensated by the measuring frequency shift or by applying an appropriate matching network at the antenna ports (not performed in this work).

It is important to note that, the measured diversity gain of the present phase-pattern diversity system is the same as the space diversity system [22], if an equivalent correlation coefficient is considered.

In Fig. 7 it was shown that the CDF plot of a single antenna compared to diversity configuration is shifted to the right. This is because, a single antenna in a multipath environment receives more mean power than coupled antennas, where the radiation efficiency is reduced by the absorption and mismatch effects [13]. To include this

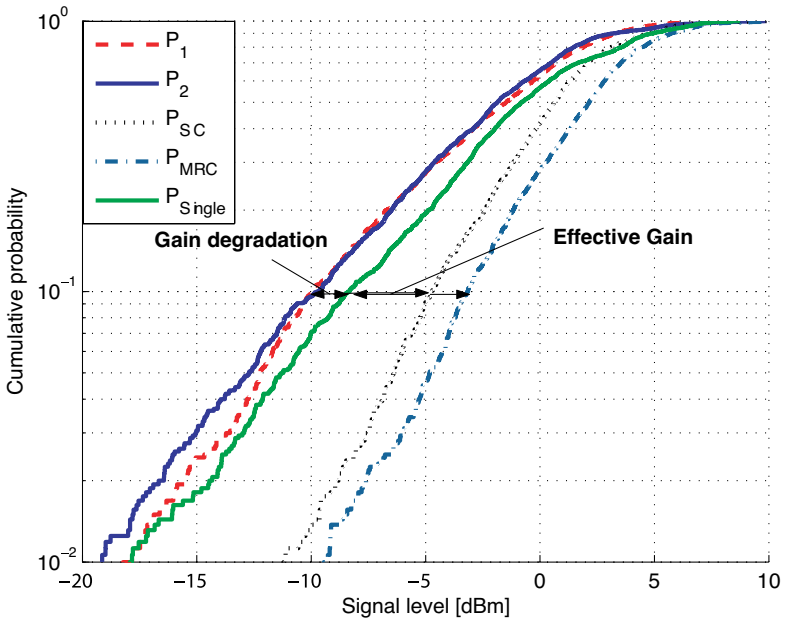

Figure 7. CDF of the measured signal powers inside reverberation chamber for dipole spacing $d = 0.2\lambda$; P_1 and P_2 are the measured signal powers in the diversity branches; P_{SC} and P_{MRC} are the signal power after diversity combining; P_{Single} is the signal power received with a single antenna with no antenna close to it.

effect in the diversity gain, we extract the gain in relation to the CDF plot of a single antenna measured at the identical propagation channels (effective diversity gain). Fig. 9 illustrates the measured effective diversity gain versus dipoles separation. As shown, the gain is smoothly reduced (about 1 dB) within 0.5λ and 0.15λ apart; in smaller distances the gain is rapidly dropped. This is a good result showing the limit of spacing between coupled antennas for effective diversity application. It can also be concluded that, a small correlation coefficient is not the sufficient condition for optimum diversity gain performance.

3.4. Antenna Efficiency

In this part we compare the modeled antenna radiation efficiency with the measured mean powers inside the reverberation chamber. The radiation efficiency is most conventionally calculated in transmit mode and it is the same on reception, due to reciprocity. In the

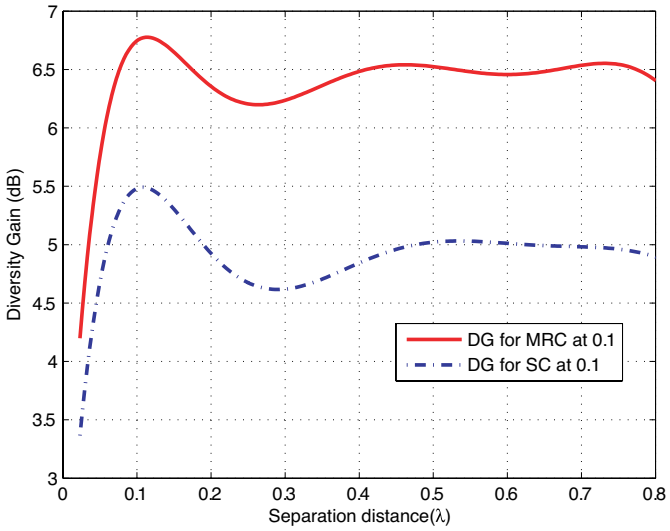

Figure 8. Measured apparent diversity gain (dB) versus dipole spacing (λ) for selection combining (SC) and maximum ratio combining (MRC) at 0.1 CDF level.

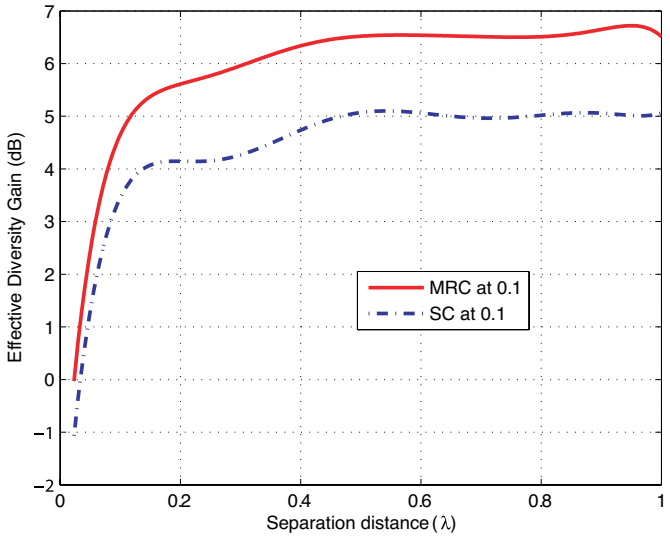

Figure 9. Measured effective diversity gain (dB) versus dipole spacing (λ) for selection combining (SC) and maximum ratio combining (MRC) at 0.1 CDF level.

coupled antennas the radiation efficiency is degraded by absorption in neighboring antenna or by impedance mismatch at the antenna terminals. The antenna efficiency for various dipole separations is calculated using TLM method by exciting one antenna and 50Ω terminating of the next antenna. Integrating the loss (material loss and power absorption at the next 50Ω terminal load) over calculating volume and considering the mismatch effects, gives the overall antenna efficiency. Antenna efficiency in diversity prototype is compared to single antenna efficiency, with no additional antenna close to it, and the overall efficiency degradation versus dipoles distance is computed and is plotted in Fig. 10.

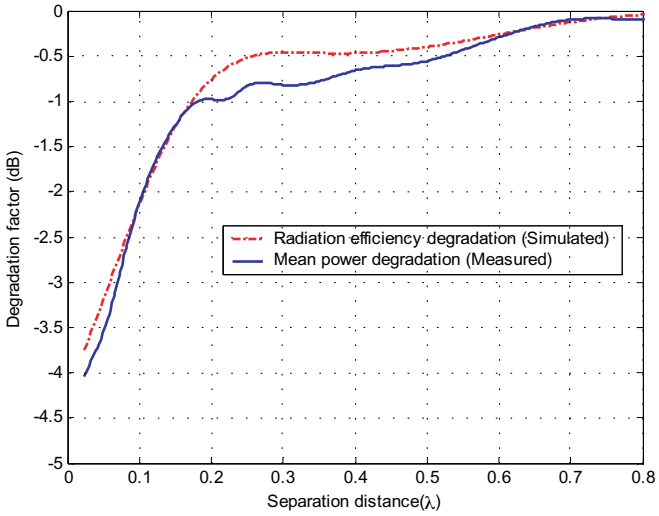

Figure 10. Simulated radiation efficiency degradation (dB) and the measured mean signal power degradation (dB) in diversity configuration compared to single dipole antenna, versus dipole spacing (λ).

The mean received powers at the fixed dipole antenna port (see Fig. 6), in diversity configuration are compared to that mean received power with no additional antenna close to it. The mean power degradation is evaluated and is depicted in Fig. 10. By comparing the two curves in Fig. 10 we conclude that the mean received power reduction, due to coupling, in diversity prototype is approximately equal to the simulated antenna efficiency degradation factor. A comparison among Figures 8–10 reveals that, the effective diversity

gain at 0.1 CDF level (Fig. 9) is equal to the difference in dB between apparent diversity gain in Fig. 8 and efficiency degradation factor in Fig. 10. The measured and simulated degradation factors are in good agreement with the measurements presented by Kildal [13].

4. CONCLUSION

This paper has presented the pattern analysis of two parallel dipoles in diversity configuration. The correlation aspects of the parallel dipoles are investigated in detail. Phase-pattern diversity is illustrated that significantly reduces the signals correlation in small dipole spacing. It was shown that, the radiation patterns can be highly overlapped but still produce uncorrelated signals in multipath environments due to their phase difference.

The diversity configuration is explored inside the multipath channel of a reverberation chamber. A measurement setup is proposed that offers a reasonable measurement time for signals acquisition. Diversity performance factors include: signals correlation coefficient, diversity gain for SC and MRC are measured. The diversity gain of the phase-pattern diversity is comparable with the diversity gain of the space diversity systems.

Mutual coupling is efficient for the signals correlation but reduces the radiation efficiency. The effective diversity gain is a good indicator gives the performance enhancement of the coupled antennas. The minimum dipole spacing for optimum gain, based upon the effective diversity gain, is measured and is about 0.15λ apart. Antenna radiation efficiency can be used for effective diversity gain estimation from the apparent diversity gain.

ACKNOWLEDGMENT

The author would like to thank Prof. Bolomey for supporting this work and also Prof. Azoulay for the discussions related to this subject. I would also like to thank Prof. P-S. Kildal for the good comments on this paper.

REFERENCES

1. Parson, J. D., *The Mobile Radio Propagation Channel*, second edition, Wiley, 2000.
2. Vaughan, R., "Spaced directive antennas for mobile communications by the Fourier transform method," *IEEE Trans. on Antennas and Propagat.*, Vol. 48, Iss. 7, 1025–1032, July 2000.

3. Balanis, C. A., *Antenna Theory: Analysis and Design*, Wiley, 1997.
4. Khaleghi, A., A. Azoulay, and J. C. Bolomey, "Diversity techniques with dipole antennas in indoor multipath propagation," *16th Annual IEEE International Symposium on Personal Indoor and Mobile Radio Communication (PIMRC)*, Berlin, Germany, Sep. 2005.
5. Vaughan, R. G. and J. B. Andersen, "Antenna diversity in mobile communications," *IEEE Trans. on Vehicular Technology*, Vol. 36, No. 4, 149–172, Nov. 1987.
6. Hui, H. T., W. T. O. Yong, and K. B. Toh, "Signal correlation between two normal-mode helical antennas for diversity reception in a multipath environment," *IEEE Trans. Antennas and Propagat.*, Vol. 52, Iss. 2, 572–577, Feb. 2004.
7. Brown, T. W. C., S. R. Saunders, and B. G. Evans, "Analysis of mobile terminal diversity antennas," *IEE Proceedings, Microwaves, Antennas and Propagation*, Vol. 152, Feb. 2005.
8. Wallace, J. W. and M. A. Jensen, "Termination-dependent diversity performance of coupled antennas: network theory analysis," *IEEE Trans. Antennas and Propagat.*, Vol. 52, Iss. 1, 98–105, Jan. 2004
9. Boyle, K., "Radiation patterns and correlation of closely spaced linear antennas," *IEEE Trans. Antennas Propagat.*, Vol. 50, 1162–1165, Aug. 2002.
10. Jensen, M. A. and Y. Rahmat-Samii, "Performance analysis of antennas for hand-held transceivers using FDTD," *IEEE Trans. Antennas Propagat.* Vol. 42, 1106–1113, Aug. 1994.
11. Leifer, M. C., "Signal correlations in coupled cell and MIMO antennas," *Proc. IEEE Antennas and Propagat. Society Int. Symp.*, Vol. 3, 194–197, June 2002.
12. Svantesson, T. and A. Ranheim, "Mutual coupling effects on the capacity of multi-element antenna systems," *Proc. IEEE ICASSP'2001*, Vol. 4, 2485–2488, May 2001.
13. Kildal, P.-S. and K. Rosengren, "Electromagnetic analysis of effective and apparent diversity gain of two parallel dipoles," *IEEE Antennas and Wireless Propagat. Letters*, Vol. 2, April 2003.
14. Rosengren, K. and P.-S. Kildal, "Radiation efficiency, correlation, diversity gain, and capacity of a six monopole antenna array for a MIMO system: Theory, simulation and measurement in reverberation chamber," *Proceedings IEE, Microwave, Antennas Propag.*, Vol. 152, No. 1, 7–16, Feb. 2005.

15. Rosengren, K. and P.-S. Kildal, "Study of distribution of modes and plane waves in reverberation chamber for characterization of antennas in multipath environment," *Microwave and Optical Technology Letters*, Vol. 30, No. 20, 386–391, Sep. 2001.
16. Khaleghi, A., J. C. Bolomey, and A. Azoulay, "On the statistics of the reverberation chambers and application for wireless antenna test," *IEEE symposium on the Antennas and Propagation (AP-S)*, Albuquerque, NM, July 2006.
17. Taga, T., "Analysis for mean effective gain of mobile antenna in land mobile radio environments," *IEEE Trans. on Vehicular Technology*, Vol. 39, No. 2, 117–131, May 1990.
18. Douglas, M. G., M. Okoniewski, and M. A. Stuchly, "A planar diversity antenna for handheld PCS devices," *IEEE Trans. on Vehicular Technology*, Vol. 47, No. 3, 747–754, Aug. 1998.
19. Glazunov, A., "Theoretical analysis of mean effective gain of mobile terminal antennas in Ricean channels," *56th IEEE Conference on VTC*, Vol. 3, 1796–1800, Fall 2002.
20. Clarke, R. H., "A statistical theory of mobile radio reception," *Bell Syst. Tech. J.*, Vol. 47, 957–1000, 1969.
21. Scott, N. L., M. O. Leonard-Taylor, and R. G. Vaughan, "Diversity gain from a single-port adaptive antenna using switched parasitic elements illustrated with a wire and monopole prototype," *IEEE Trans. Antennas and Propagat.*, Vol. 47, 1066–1070, June 1999.
22. Mattheijssen, P., M. H. A. J. Herben, G. Dolmans, and L. Leyten, "Antenna-pattern diversity versus space diversity for use at handhelds," *IEEE Trans.s on Vehicular Technology*, Vol. 53, Iss. 4, 1035–1042, July 2004.
23. Khaleghi, A., J. C. Bolomey, and A. Azoulay, "A pattern diversity antenna with parasitic switching elements for wireless LAN communications," *2nd IEEE International Symposium on Wireless Communication Systems 2005 (ISWCS2005)*, Siena, Italy, 2005.
24. Clarke, R. H., "A statistical theory of mobile-radio reception," *Bell Syst. Tech. J.*, 957–1000, July–Aug. 1968.
25. Jakes, W. C., *Microwave Mobile Communications*, IEEE Press, Piscataway, NJ, 1994.
26. Kouveliotis, N. K., P. T. Trakadas, and C. N. Capsalis, "FDTD modelling of a vibrating intrinsic reverberation chamber," *Journal of Electromagnetic Waves and Applications*, Vol. 17, 849–850, 2003.

27. Musso, L., F. Canavero, B. Démoulin, and V. Bérat, *A Plane Wave Monte-Carlo Simulation Method for Reverberation Chamber*, EMC Europe, Sorrento, Italy, 2002.